DOI https: //doi. org/10.1007/s11595-023-2740-2

Tailoring Carbon Distribution in α/γ Phase of Ductile Iron and Its Effects on Thermal Conductivity

LIU Chen[1], DU Yuzhou[1*], YING Tao[2], ZHANG Liandong[3], ZHANG Xinyu[1], DONG Dan[1], JIANG Bailing[1]

(1. School of Materials Science and Engineering, Xi'an University of Technology, Xi'an 710048, China; 2. School of Materials Science and Engineering, Shanghai Jiao Tong University, Shanghai 200240, China; 3. The Second Affilated Hospital of Xi'an Jiaotong University, Xi'an 710004, China)

Abstract: The effects of carbon distribution on the microstructure and thermal conductivity of ductile iron were investigated in the present study. The microstructure of as-cast and quenched ductile iron were characterized by OM and SEM. Results showed that the microstructure of as-cast ductile iron was composed of spheroidal graphite, ferrite with the volume of 80%, and a small amount of pearlite, and quenched ductile iron was composed of spheroidal graphite, coarse/fine acicular martensite (α_M phase) and high-carbon retained austenite (γ phase). The volume fraction of retained austensite and its carbon content for direct quenched ductile iron and tepmered ductile iron were quantitatively analysed by XRD. Results revealed that carbon atoms diffused from α_M phase to γ phase during tempering at low temperatures, which resulted in carbon content in retained γ phase increasing from 1.2 wt% for the direct quenched sample to about 1.9 wt% for the tempered samples. Consequently, the lattice distortion was significantly reduced and gave rise to an increase of thermal conductivity for ductile iron.

Key words: ductile iron; carbon distribution; retained austenite; thermal conductivity; lattice distortion

1 Introduction

The mechanical properties improvement of ductile iron[1] has attracted researchers' attention because the spheroidal graphite reduces stress concentration and gives rise to an acceptable ductility[2]. The heat treatment of steels was commonly applied to improve the mechanical properties of ductile iron[3]. For example, isothermal treatment at a temperature above Ms was conducted on ductile iron, which gave rise to an ausferrite microstructure and a good mechanical property[4]. The previous investigations of steels and ductile iron indicated that carbon distribution is a critical factor to determine mechanical properties[5,6]. For example, partitioning treatment promoted carbon atoms diffusion from α phase to γ phase of austempered ductile iron (ADI) and resulted in a significant enhancement of ductility[7]; a microstructure with martensite and carbon-rich retained austenite obtained via quenching and partitioning (Q&P) treatment in ductile iron exhibited a tensile strength of 1 450 MPa and elongation of 2.2%[8].

It should be noted that the major merit of ductile iron compared with forged steels is its good self-lubricating property because of the existence of graphite[9]. Therefore, ductile iron is a preferred candidate to replace forged steels in the field of transmission parts such as automotive crankshafts, bearings, gears[10,11]. Additionally, large amount of heat produced during service would result in a rapid increase of temperature to 300-700 ℃ on the tribosurface and cause softness[12], which is an important reason for the failure of transmission parts, especially under high speed and high load service conditions. Therefore, high thermal conductivity accelerating the diffusion of heat generated during service can slow down the increase of temperature and eventually enhance service life of transmission parts.

The thermal conductivity of ductile iron is commonly higher than that of steel because of the existence of graphite[13]. Additionally, the matrix of ductile iron plays an important role in thermal conductivity[14]. Generally, thermal conductivity consists of electron thermal conductivity and phonon thermal conductivity[15] and

(Received: Mar. 29, 2022; Accepted: Jan. 18, 2023)

LIU Chen (刘琛): Ph D; E-mail: 2411245439@qq.com

*Corresponding author: DU Yuzhou (杜玉洲): Prof.; Ph D; E-mail: duyuzhou@xaut.edu.cn

Funded by China Postdoctoral Science Foundation (Nos. 2019M653703 and 2020T130523) and Xi'an University of Technology Youth Nova Fund (No. 101-451320005)

it is determined by thermal resistance, which contains phonon thermal resistance including phonon-phonon, phonon-defect, phonon-electron scattering, and electron thermal resistance including electron-defect, and electron-phonon scattering[13]. It is known that carbon atoms in Fe matrix has an obvious influence on the distortion degree of Fe lattice[16], which directly affects the scattering degree of phonon and electron and then causes the variation of thermal conductivity. Hence, tailoring carbon distribution might be an effective method to enhance the thermal conductivity of ductile iron. Though the previous investigations improved the mechanical properties of ductile iron by tailoring carbon distribution[7,17], the thermal conductivity was seldom been studied. Therefore, the present study mainly focused on the correlationship between the thermal conductivity and carbon distribution of ductile iron. The carbon distribution of ductile iron was tailored by quenching and tempering heat treatment and its effects on thermal conductivity were investigated.

2 Experimental

The material used in this work was a cylindrical ductile iron casting with a diameter of 180 mm, which was fabricated by horizontal continuous casting. The detailed casting process could be referred to the previous literature[18]. The chemical composition of as-cast ductile iron used in this study was given in Table 1.

Table 1 Chemical compositions of the ductile iron

C	Si	Mn	S	P	Mg	RE	Fe
3.55-3.85	2.34-2.86	<0.6	<0.025	<0.08	0.02-0.04	0.03-0.05	Bal.

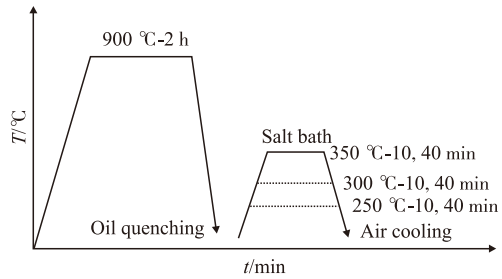

Fig.1 Scheme of heat treatments

Due to different cooling rates during solidification, the count of nodular graphite is different along radial direction. In order to eliminate the influence of spheroidal graphite on the thermal conductivity of ductile iron, all the samples used in the present study with a size of 10 mm × 20 mm × 70 mm were cut from the outside of the cylindrical profile.

The as-cast samples were firstly heated to 900 ℃ and kept for 2 h, and then quenched into oil. After that, the quenched samples were tempered at 250, 300 and 350 ℃ in a salt bath consisting of 50% $NaNO_3$ and 50% $NaNO_2$ for 10 min and 40 min, respectively, and finally air-cooled to room temperature. The heat treatment process was shown in Fig.1.

Microstructures of the samples were characterized by OLYMPUS GX71 optical microscope (OM) and JSM-6700F scanning electron microscopy (SEM) with an accelerating voltage of 30 kV. The as-cast and heat-treated samples for OM and SEM were machined and polished, and then etched by 4% nital solution. The nodular graphite count of ductile iron was calculated using the software of Image J. XRD was conducted on an XRD-7000 diffractometer with a scanning angle from 35° to 90° and the scanning speed was 4°/ min. The (200) and (211) diffraction peaks of α phase and (200) and (220) diffraction peaks of γ phase were selected to calculate the volume fraction. The volume fraction of retained austenite was calculated using the following equation[19]:

$$V_\gamma = \frac{1}{1 + G(I_\alpha / I_\gamma)} \quad (1)$$

where V_γ represents the volume fraction of retained austenite (wt%); I_α and I_γ represent the integral strength of diffraction peak of ferrite/martensite and austenite, respectively; G is the ratio of intensity-related factors corresponding to each diffraction plane of austenite and ferrite/martensite. According to the previous literature, the G values of the diffraction peaks corresponding to $I_\alpha(200)/I_\gamma(200)$, $I_\alpha(200)/I_\gamma(220)$, $I_\alpha(211)/I_\gamma(200)$, $I_\alpha(211)/I_\gamma(220)$ are 2.5, 1.38, 1.19, 0.6, respectively[20].

In order to calculate the carbon content in retained austenite, the $(200)_\gamma$ diffraction peak of retained austenite corresponding to the diffraction angle from 48° to 52° was scanned with the scanning speed of 0.2 °/min. The carbon content in retained austenite was calculated using Eq.(2)[21].

$$a_\gamma = 0.354\,8 + 0.004\,4C_\gamma \quad (2)$$

where a_γ is the lattice constant of retained austenite (nm) which was calculated based on the $(200)_\gamma$ diffraction peaks of retained austenite and C_γ represents the carbon content of austenite (wt%).

The disk-shaped samples with the size of Φ 12.7×1.5 mm were cut from the heat-treated samples in order to measure its thermal diffusivity. The thermal diffusivity was measured at 20, 100, 150, 200, 250 and 300 ℃ using a Netzsch 447 apparatus via laser flash

method. The samples were tested three times at each temperature and then the average value was taken. Thermal conductivity λ was calculated by thermal diffusivity using the following equation[13]:

$$\lambda = D \cdot C_p \cdot \rho \tag{3}$$

where λ is the thermal conductivity ($W \cdot m^{-1} \cdot k^{-1}$) and D is the thermal diffusivity coefficient ($m^2 \cdot s^{-1}$). C_p is the specific heat ($J \cdot kg^{-1} \cdot k^{-1}$) and ρ is the density ($kg \cdot m^{-3}$). The constant pressure heat capacity C_p is a parameter insensitive to impurities and structure, hence the value measured by a Netzsch DSC 404 C Pegasus differential scanning is used[22]. The density of the samples at room temperature were obtained by Archimedes method. The density were calculated by the following equation with temperature rising[23]:

$$\rho_\gamma = \frac{\rho_{RT}}{1 + 3\alpha\Delta T} \tag{4}$$

where α is the coefficient of thermal expansion, and here $\alpha = 14.5 \times 10^{-6}$ was used[22]. ρ_{RT} is the density of the samples at room temperature and ΔT is the temperature difference between T and 20 ℃.

3 Results

3.1 Microstructure

Fig.2 shows the SEM images of the as-cast sample. It can be seen that the cast ductile iron was consisted of nodular graphite, ferrite and pearlite, in which the nodular graphite was uniformly distributed around the matrix. The count of nodular graphite was estimated to be about 300 mm^2. Ferrite with the volume fraction of 80% distributed around the nodular graphite (Fig.2(a)), which was a typical microstructure of as-cast ductile iron[24].

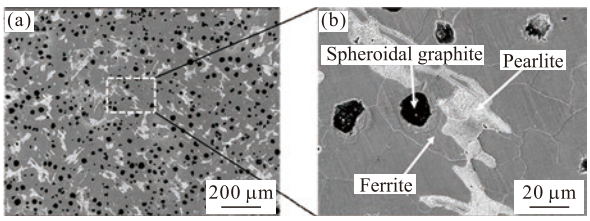

Fig.2 SEM images of the as-cast ductile iron with (a) low and (b) high magnification

Fig.3 shows OM images of ductile iron after heat treatment. All the samples were composed of acicular martensite with a dark contrast and retained austenite with white contrast. The acicular martensite included fine acicular martensite and coarse acicular martensite, in which fine acicular martensite mainly distributed in the vicinity of spheroidal graphite. Additionally, all the samples showed a similar amount of martensite and retained austenite except the sample tempered at 250 ℃ for 10 min.

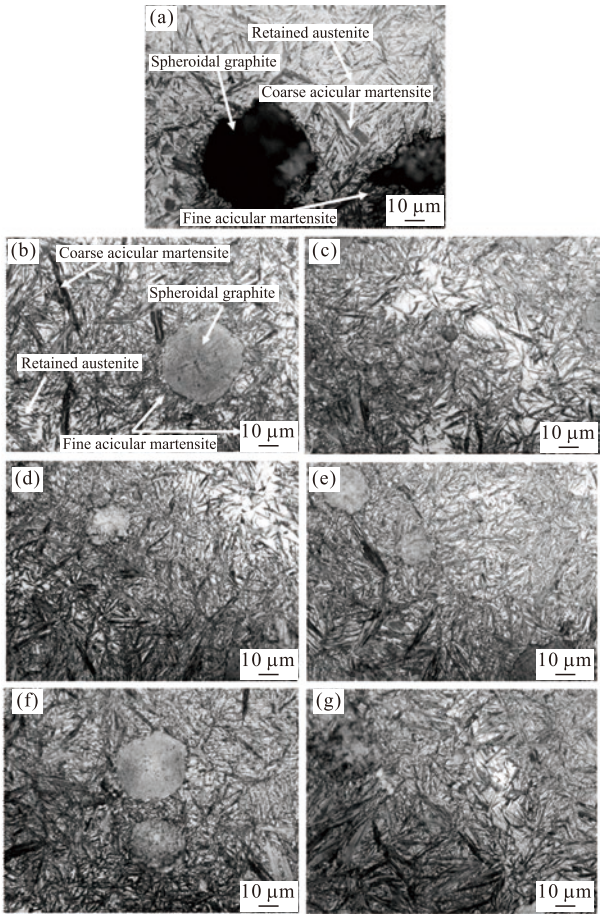

Fig.3 Optical images of the (a) quenched and (b-g) tempered samples at (b) 250 ℃; (d) 300 ℃; (f) 350 ℃ for 10 min and at (c) 250 ℃, (e) 300 ℃, (g) 350 ℃ for 40 min

Fig.4 shows the SEM images of the heat-treated samples. The coarse acicular martensite with an average thickness of 1.29±0.04 μm and fine acicular martensite with an average thickness of 0.26±0.08 μm could be clearly observed. No obvious difference in the size of martensite was detected for the tempered samples. The coarsely lenticular martensite with a ridge in the middle was observed for the quenched and tempered samples (Fig.4(b)). The volume fraction of coarse martensite was about 30% and the fine acicular martensite was about 40%. The retained austenite exhibited two different morphologies: blocky austenite and filmy austenite distributing between fine acicular martensite (Fig.4(c)). The amounts of fine acicular martensite and filmy austenite increased with the increase of tempering temperature and time, while the amount of blocky austenite was reduced. It is commonly accepted that

the blocky austenite contained less carbon atoms compared with the filmy austenite[25]. Therefore, the blocky austenite was more unstable, which might transform to bainite during tempering and resulted in the reduction of blocky austenite. It should be noted that no carbides were detected for all the samples, indicating that the supersaturated carbon in the martensite did not form carbides during tempering.

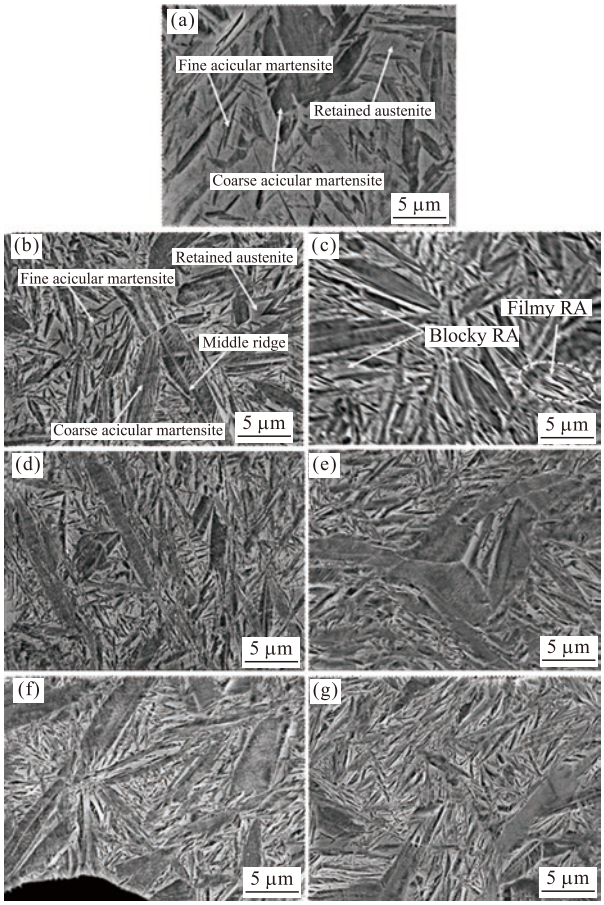

Fig.4 SEM images of the (a)quenched sample and (b-g) samples tempered at (b) 250 ℃, (d) 300 ℃, (f) 350 ℃ for 10 min and at (c) 250 ℃, (e) 300 ℃, (g) 350 ℃ for 40 min

Fig.5 shows the XRD patterns of the samples. The diffraction peaks of α and γ phases were observed, indicating that all the samples after heat treatment were composed of α and γ phases, which was consistent with the results observed by OM and SEM. The retained austenite peak of the tempered sample at 250 ℃ for 10 min was weaker compared with other samples. It was inferred that the retained austenite might be unstable after tempering at 250 ℃ for 10 min and transformed to other phases during cooling to room temperature, which would be discussed in the following.

The volume fraction of retained austenite after tempering is shown in Fig.6. The volume of retained austenite in the tempered samples was similar except that tempered at 250 ℃ for 10 min. The volume fraction of retained austenite for sample tempered at 250 ℃ for 10 min was about 15.4%, while the value for other tempered samples was about 21.0%.

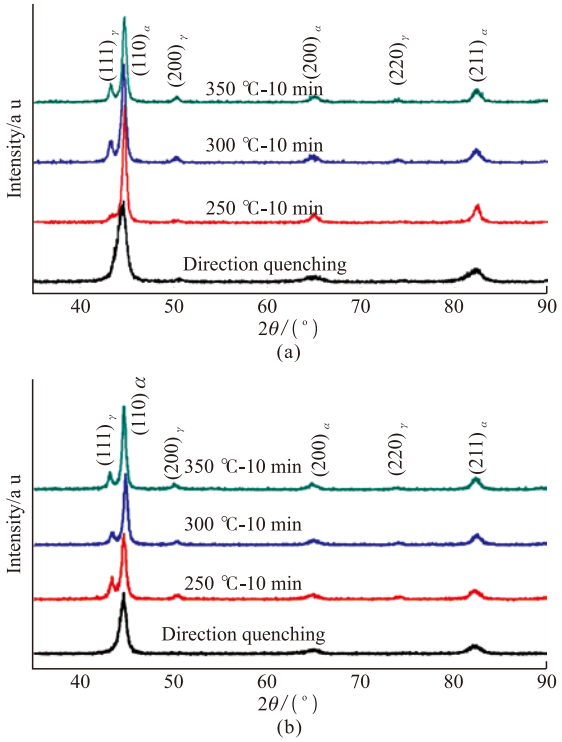

Fig.5 XRD patterns of the samples tempered for (a) 10 min and (b) 40 min

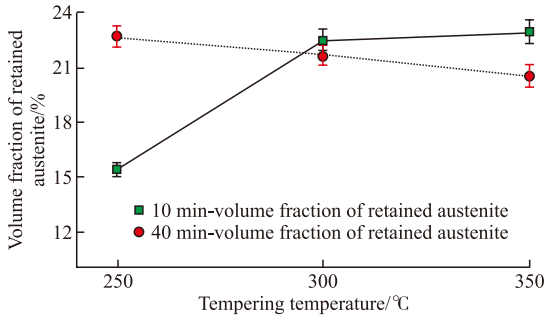

Fig.6 The variation of volume fraction of retained austenite with tempering temperature

In order to further investigate carbon atoms diffusion during tempering process, the $(200)_\gamma$ peaks of XRD patterns were measured with a small step size, which was presented in Fig.7. It could be clearly seen that the $(200)_\gamma$ peaks of the tempered samples shifted towards a small angle compared with that of the quenched sample, indicating that carbon atoms diffused from martensite to retained austenite during tempering and led to the supersaturated carbon atoms concentration in retained austenite. However, the deviation degree was different for samples tempered at different conditions. The samples tempered at 300 and 350 ℃

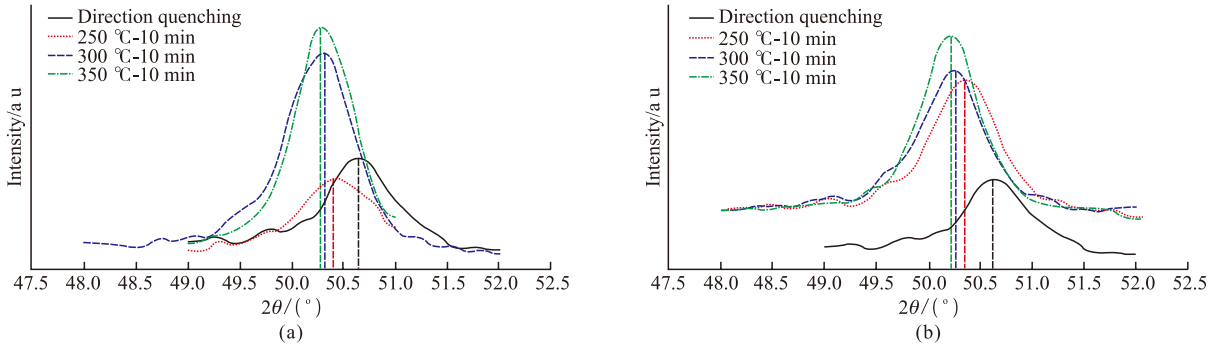

Fig.7 The $(200)_{\gamma}$ peaks of XRD patterns of the samples tempered for (a) 10 min and (b) 40 min

exhibited a similar $(200)_{\gamma}$ diffraction angle, indicating that the carbon diffusion from supersaturated α phase to retained γ phase almost reached an equilibrium state when tempered at temperature higher than 300 ℃.

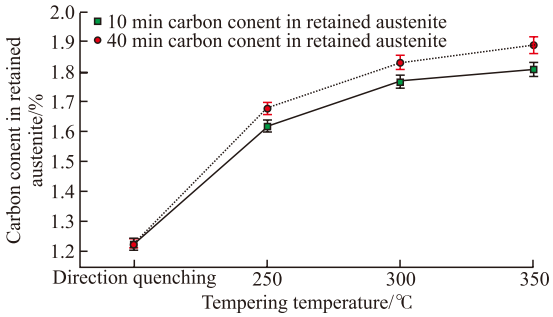

Fig.8 The variation of carbon content in retained austenite with tempering temperature

According to the XRD results, the carbon content in retained austenite is calculated (Fig.8). The carbon content in retained austenite increased from 1.23% for quenched sample to 1.81% for sample tempered at 350 ℃ for 10 min, indicating carbon atoms diffusion from martensite to retained austenite. In addition, the carbon content in retained austenite was increased with increasing tempering time. The value was increased from 1.77% for sample tempered at 300 ℃ for 10 min to 1.83% for that for 40 min. The tempered sample at 250 ℃ for 10 min contained the lowest carbon content in retained austenite.

3.2 Thermal conductivity

Fig.9 shows the variation of thermal conductivity with temperature. The thermal conductivity increased with the increase of temperature from 20 to 300 ℃. The thermal conductivity of the quenched sample was the lowest at the temperature lower than 150 ℃. Tempering effectively improved the thermal conductivity of ductile iron under low temperature (<150 ℃). The thermal conductivity of the samples tempered at 300 and 350 ℃ were similar. However, the tempered samples

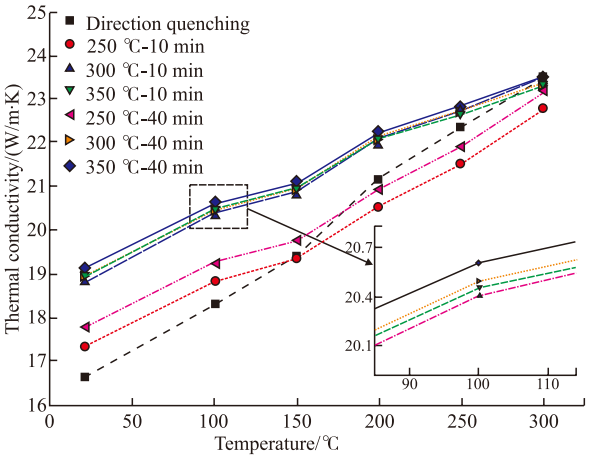

Fig.9 The variation of thermal conductivity of ductile iron with temperature

at 250 ℃ exhibited a lower thermal conductivity compared with other tempered samples. With the increase of temperature, when the temperature is higher than 200 ℃, the thermal conductivity of the quenched sample was higher than that of the sample tempered at 250 ℃. Interestingly, all the samples exhibited a similar thermal conductivity at 300 ℃ except for the sample tempered at 250 ℃ for 10 min.

4 Discussion

The effects of carbon distribution on the microstructure and thermal conductivity of ductile iron were studied. Tempering treatment promoted carbon atoms to diffuse from supersaturated α_{M} phase to γ phase, which resulted in the microstructure change and then affected the thermal conductivity. The microstructure evolution and mechanisms of thermal conductivity are discussed as follows.

4.1 Microstructure evolution during tempering treatment

The matrix microstructure of quenched ductile iron was composed of acicular martensite and retained

austenite. During tempering treatment, carbon atoms diffused from supersaturated α_M phase to γ phase because of the difference of chemical potential of carbon atoms in α_M and γ phase, resulting in the increase of carbon concentration of retained austenite but did not result in the formation of carbide due to existence of high silicon[26]. Consequently, α_M phase and carbon-supersaturated γ phase were obtained.

It should be noted that carbon diffusion varied when tempering at different temperatures. The diffusion rate of carbon atoms increased with the increase of tempering temperature. Therefore, more carbon content was detected in the retained austenite of the samples tempered at higher temperature (Fig.8). When the tempering temperature was higher than 300 ℃, the carbon diffusion reached equilibrium state even for a short time. Therefore, the samples tempered at 300 and 350 ℃ had a similar carbon content in retained austenite. However, for the samples tempered at 250 ℃, the diffusion velocity of carbon atom was not fast enough to reach equilibrium state when tempering for a short time, which resulted in a smaller carbon content in retained austenite. However, prolonging tempering time gave more time for diffusion of carbon, which led to an increase of carbon content in retained austenite for sample tempered at 250 ℃ for 40 min.

Additionally, the carbon content in austenite directly determined the stability of retained austenite[25]. The increase of carbon content could stabilize the retained austenite. Consequently, the samples tempered at high temperature with high carbon content in retained austenite exhibited a stable microstructure and the retained austenite was remained. However, for the sample tempered at 250 ℃ for 10 min, low carbon content in retained austenite resulted in the phase transformation during cooling to temperature and led to an obvious decrease of retained austenite (Fig.6).

4.2 Thermal conductivity analysis

The ductile iron in the present study exhibited obvious difference in thermal conductivity under different states. The factor affecting thermal conductivity is thermal resistance containing phonon thermal resistance and electron thermal resistance[13]. The point defects in the crystal increased was high at high temperature, which would increase the probability of collision between phonons and phonons as well as electrons and electrons[27] and would deteriorated the thermal conductivity. However, high temperature increased the heat capacity and velocity of phonons and electrons, which was beneficial for the increase of thermal conductivity[28]. The final change of the thermal conductivity with temperature relied on the superposition of the two cases and the latter situation prevailed in the temperature range of 20-300 ℃ for ductile iron[29]. Consequently, the thermal conductivity increased with the increase of temperature (Fig.9).

It is known that carbon atoms mainly exist in the octahedral lattice gaps of iron atoms. α-Fe is body-centered cubic structure and its octahedral gap radius is only 0.067 Å. γ-Fe has a face-centered cubic structure and its octahedral gap radius is 0.146 Å. Hence, the lattice distortion caused by carbon atoms in γ phase was much smaller than that in α phase. Large lattice distortions would increase the scattering of phonons and electrons, resulting in the decrease of thermal conductivity[15]. Consequently, tempering treatment effectively increased the thermal conductivity because more carbon atoms existed in γ phase for the tempered samples. In addition, with the increase of tempering temperature from 250 to 300 ℃, the diffusion of carbon atoms from α phase to γ phase is faster in the samples, then the diffusion of carbon atoms becomes slower and finally tends to equilibrium at the sample tempered at 350 ℃ (Fig.7), which leads to lower thermal conductivity at 250 ℃ for 10 min and 40 min, then a larger increase in thermal conductivity for the samples tempered at 300 ℃. And the thermal conductivity finally tends to be close when the samples tempered at 300 and 350 ℃ (Fig.9).

It should be noted that the increase of thermal conductivity for the tempered samples compared with the quenched sample was reduced with the increase of temperature (Fig.9). The coefficient of thermal expansion of the material increased with the increase of temperature[30]. Therefore, the distance between Fe atoms became larger at high temperature, which caused the decrease of the lattice distortion induced by the interstitial carbon atoms. As a result, the distribution of carbon atoms in α_M or γ phase has a negligible effect on thermal conductivity at high temperature. It could be seen that all the samples at 300 ℃ exhibited a similar thermal conductivity.

In addition, when the measured temperature was higher than 200 ℃, the thermal conductivity of the quenched sample was higher than that of the sample tempered at 250 ℃, which might be closely related to the content of retained austenite. When the measured temperature was low, carbon distribution played a leading role in the effect of thermal conductivity. However, when the measured temperature was higher than 200 ℃,

the unstable retained austenite in the sample tempered at 250 ℃ would be transformed into martensite, which lead to the thermal conductivity of the sample tempered at 250 ℃ to be lower than that of the quenched sample and the specific change mechanism of thermal conductivity needs to be further studied.

5 Conclusions

a) The microstructure of ductile iron after quenching and tempering treatment is composed of coarse acicular martensite, fine acicular martensite and retained austenite.

b) The diffusion of carbon atoms from martensite to retained austenite occurred during tempering treatment due to the existence of high silicon in ductile iron.

c) The thermal conductivity of ductile iron at low temperature increases with the increase of tempering temperature, which is mainly related to the distribution of carbon atoms.

d) The thermal conductivity differed little at high temperature because the lattice distortion caused by the solutionized carbon atoms in α_M and γ phase has no obvious difference.

Conflict of interest

All authors declare that there are no competing interests.

References

[1] Dhanasekaran S, Vadiraj A, Balachandran G, *et al.* Mechanical Behaviour of an Austempered Ductile Iron[J]. *T. Indian I. Metals*, 2010, 63(5): 779-785

[2] Ghassemali E, Hernando J C, Stefanescu D M, *et al.* Revisiting the Graphite Nodule in Ductile Iron[J]. *Scripta Mater*., 2019, 161: 66-69

[3] Chen L S, Hu B J, Xu J H, *et al.* Cu Partitioning Behavior and Its Effect on Microstructure and Mechanical Properties of 0.12C-1.33Mn-0.55Cu Q&P Steel[J]. *J. Wuhan. Univ. Technol. -Materials Science Edition*, 2017, 32(5): 1 179-1 185

[4] Dakre V, Peshwe D R, Pathak S U, *et al.* Mechanical Characterization of Austempered Ductile Iron Obtained by two Step Austempering Process[J]. *T. Indian I. Metals*, 2017, 70(9): 2 381-2 387

[5] Zhang M Y, Zhu F X, Duan Z T, *et al.* Characteristics of Retained Austenite in TRIP Steels with Bainitic Ferrite Matrix[J]. *J. Wuhan. Univ. Technol. -Materials Science Edition*, 2011, 26(6): 1 148-1 151

[6] Nishikawa A S, Miyamoto G, Furuhara T, *et al.* Phase Transformation Mechanisms during Quenching and Partitioning of a Ductile Cast Iron[J]. *Acta Mater*., 2019, 179: 1-16

[7] Wang X, Du Y, Liu B, *et al.* Enhanced Plasticity of Austempered Ductile Iron (ADI) by Partitioning Treatment[J]. *Mater. Sci. Eng. A*, 2021, 804: 140 513

[8] Melado A C, Nishikawa A S, Goldenstein H, *et al.* Effect of Microstructure on Fatigue Behaviour of Advanced High Strength Ductile Cast Iron Produced by Quenching and Partitioning Process[J]. *Int. J. Fatigue*, 2017, 104: 397-407

[9] Akinribide O J, Akinwamide S O, Obadele B A, *et al.* Tribological Behaviour of Ductile and Austempered Grey Cast Iron under Dry Environment[J]. *Materials Today: Proceedings*, 2020, 38: 1 174-1 182

[10] Du Y, Wang X, Zhang D, *et al.* A Superior Strength and Sliding-Wear Resistance Combination of Ductile Iron with Nanobainitic Matrix[J]. *J. Mater. Res. Technol*., 2021, 11: 1 175-1 183

[11] Sazegaran H, Kiani-Rashid A-R, Khaki J V. Effects of Sphere Size on the Microstructure and Mechanical Properties of Ductile Iron-Steel Hollow Sphere Syntactic Foams[J]. *Int. J. Min. Met. Mater*., 2016, 23(6): 676-682

[12] Quinn T F J. The Effect of "Hot-Spot" Temperatures on the Unlubricated Wear of Steel[J]. *A S L E Trans*., 1967, 10(2): 158-168

[13] Holmgren D. Review of Thermal Conductivity of Cast Iron[J]. *Inter. J. Cast Metals Res*., 2005, 18(6): 331-345

[14] Rukadikar M C, Reddy G P. Influence of Chemical Composition and Microstructure on Thermal Conductivity of Alloyed Pearlitic Flake Graphite Cast Irons[J]. *J. Mater. Sci*., 1986, 21(12): 4 403-4 410

[15] Williams R K, Yarbrough D W, Masey J W, *et al.* Experimental Determination of the Phonon and Electron Components of the Thermal Conductivity of Bcc Iron[J]. *J. Appl. Phys*., 1981, 52(8): 5 167-5 175

[16] Xiao L, Fan Z, Jinxiu Z, *et al.* Lattice-Parameter Variation with Carbon Content of Martensite: X-ray-diffraction Experimental Study[J]. *Phys. Rev. B*, 1995, 52(14): 9 970-9 978

[17] Zhang K, Zhang M, Guo Z, *et al.* A New Effect of Retained Austenite on Ductility Enhancement in High-strength Quenching-Partitioning–Tempering Martensitic Steel[J]. *Mater. Sci. Eng. A*, 2011, 528(29): 8 486-8 491

[18] Yan G, Xu Y, Jiang B. The Production of High-density Hollow Cast-Iron Bars by Vertically Continuous Casting[J]. *J. Mater. Process. Technol*., 2012, 212(1): 15-18

[19] Wang C Y, Shi J, Cao W Q, *et al.* Characterization of Microstructure Obtained by Quenching and Partitioning Process in Low Alloy Martensitic Steel[J]. *Mater. Sci. Eng. A*, 2010, 527(15): 3 442-3 449

[20] Wen F, Zhao J, Zheng D, *et al.* The Role of Bainite in Wear and Friction Behavior of Austempered Ductile Iron[J]. *Materials*, 2019, 12(5): 767-779

[21] Roberts C S. Effect of Carbon on the Volume Fractions and Lattice Parameters of Retained Austenite and Martensite[J]. *J. Metalcast.*, 1953, 5(2): 203-204

[22] Selin M. Tensile and Thermal Properties in Compacted Graphite Irons at Elevated Temperatures[J]. *Metall. Mater. Trans. A*, 2010, 41(12): 3 100-3 109

[23] Holmgren D M, Diószegi A, Svensson I L. Effects of Transition from Lamellar to Compacted Graphite on Thermal Conductivity of Cast Iron[J]. *Inter. J. Cast Metals Res*., 2006, 19(6): 303-313

[24] Shinde V D, Ravi B, Narasimhan K. Solidification Behaviour and Mechanical Properties of Ductile Iron Castings with Varying Thickness[J]. *Inter. J. Cast Metals Res*., 2012, 25(6): 364-373

[25] De Moor E, Lacroix S, Clarke A J, *et al.* Effect of Retained Austenite Stabilized via Quench and Partitioning on the Strain Hardening of Martensitic Steels[J]. *Metall. Mater. Trans. A*, 2008, 39(11): 2 586-2 595

[26] Vélez J M, Garboggini A, Tschiptschin A P. Effect of Silicon on Kinetics of Bainitic Reaction in Austempered Ductile Cast Iron[J]. *Mater. Sci. Technol*., 1996, 12(4): 329-337

[27] Williams R K, Graves R S, Weaver F J, *et al.* Effect of Point Defects on the Phonon Thermal Conductivity of Bcc Iron[J]. *J. Appl. Phys*., 1987, 62(7): 2 778-2 783

[28] Fan H Y, Tang Z H, Li W, *et al.* The Influence of Temperature on the Thermal Conductivity of Cast Irons[J]. *Mater. Rev*., 1996, 3: 23-25

[29] Matsushita T, Saro A G, Elmquist L, *et al.* On the Specific Heat and Thermal Diffusivity of CGI and SGI Cast Irons[J]. *Int. J. Cast Metals Res*., 2017, 30(5): 276-282

[30] Çelik G A, Tzini M-I T, Polat Ş, *et al.* Thermal and Microstructural Characterization of a Novel Ductile Cast iron Modified by Aluminum Addition[J]. *Int. J. Min. Met. Mater*., 2020, 27(2): 190-199